Demons in the North Atlantic: Variability of deep ocean ventilation

G. A. MacGilchrist[1], H. L. Johnson[2], C. Lique[3], D. P. Marshall[4]

[1]Program in Atmospheric and Oceanic Science, Princeton University, Princeton, N.J., U.S.A.
[2]Department of Earth Sciences, University of Oxford, Oxford, U.K.
[3]Univ. Brest, CNRS, IRD, Ifremer, Laboratoire dOcéanographie Physique et Spatiale (LOPS), IUEM, Brest, France
[4]Department of Physics, University of Oxford, Oxford, U.K.

Key Points:

- Temporal variability of high-latitude ocean ventilation is investigated using Lagrangian trajectories in an eddy-permitting ocean model.
- High-latitude ocean ventilation adheres to "Stommel's Demon", such that only water subducted in late winter is retained in the subsurface.
- An interannual Demon also operates to mediate exchange between the atmosphere and subsurface ocean on longer timescales.

Corresponding author: Graeme A. MacGilchrist, graemem@princeton.edu

Abstract

Translation of atmospheric forcing variability into the ocean interior via ocean ventilation is an important aspect of transient climate change. On a seasonal timescale, this translation is mediated by a so-called "Demon" that prevents access to all except late-winter mixed-layer water. Here, we use an eddy-permitting numerical circulation model to investigate a similar process operating on longer timescales in the high-latitude North Atlantic, which we denote the "interannual Demon". We find that interannual variations in atmospheric forcing are indeed mediated in their translation to the ocean interior. In particular, the signature of persistent strong atmospheric forcing driving deep mixed layers is preferentially ventilated to the interior when the forcing is ceased. Susceptibility to the interannual Demon depends on the location and density of subduction — with the rate at which newly ventilated water escapes its region of subduction being the crucial factor.

Plain Language Summary

Water that leaves the ocean's surface boundary layer — where water is in direct contact with the overlying atmosphere — to be transported into the subsurface, is said to be "ventilated" (the name arising from the abundance of oxygen in newly ventilated water). The ventilation process, which carries implications for the ocean storage of climate-relevant substances such as carbon dioxide, occurs only at certain times and under certain conditions. In describing a mechanism for the selective nature of ventilation over the seasonal cycle, Henry Stommel imagined a Demon sitting at the base of the surface boundary layer, granting access only to parcels of water that meet certain characteristics (namely their speed of "escape"). Thus, "Stommel's Demon" was born. Here, we investigate this same process as it operates in more northerly regions and on longer timescales. In so doing we give birth to a new "interannual Demon", and describe its characteristics.

1 Introduction

In 1939, Iselin noted that the properties of the ocean thermocline match those of the late winter mixed layer, as opposed to a year-round average (Iselin, 1939). Some forty years later, Stommel (1979) suggested that this arises from the seasonality of the mixed layer depth, which effectively re-entrains water subducted at any time except late winter. Stommel likened the process to that of "Maxwell's Demon" in thermodynamics, with the Demon here operating a trapdoor at the base of the mixed layer, allowing access to the ocean interior only for water moving away fast enough to escape re-entrainment. Williams et al. (1995) subsequently used tracers in a numerical simulation to show that this process does indeed operate as Stommel described. The process, which has since become known as "Stommel's Demon", allows for the simplification of models of the ocean thermocline, whereby the late-winter mixed layer base can be adopted as the upper boundary and mixed layer seasonality effectively ignored (Luyten et al., 1983; Sarmiento, 1983; Williams, 1991; Qiu & Huang, 1995; D. Marshall & Marshall, 1995; D. Marshall, 1997).

Here, we continue in the Demonic tradition by considering whether a similar process operates on an interannual timescale in the ventilation of deep ocean watermasses, and mediates the translation of atmospheric forcing variability into the ocean subsurface. We focus our attention on the North Atlantic, and in particular on the Labrador Sea, a critical region for the ventilation of the deep waters of the global ocean (Rhein et al., 2017; MacGilchrist et al., 2020). Water subducted here flows southward as part of the Atlantic Meridional Overturning Circulation, returning to the surface predominantly in the Southern Ocean, after a timescale on the order of centuries (DeVries & Primeau, 2011; Gebbie & Huybers, 2012). Consequently, the region has been shown to play a crucial role in transient climate change through the uptake of anthropogenic carbon diox-

ide (Khatiwala et al., 2009), oxygen (Koelling et al., 2017), and heat (Zanna et al., 2019). Understanding the sensitivity of deep ocean ventilation to changes in surface forcing is thus an important step toward accurately projecting its future evolution (Boer et al., 2007; Katavouta et al., 2019).

The North Atlantic Oscillation (NAO) is the dominant mode of atmospheric variability over the North Atlantic Ocean (Hurrell, 1995; J. Marshall et al., 2001). Identified as an oscillation in the pressure systems over Iceland and the Azores, the system swings between positive and negative phases on an approximately 3 to 7 year timescale (Hurrell & Deser, 2010). In its positive phase, the atmospheric circulation is anomalously strong and stormy, driving enhanced heat loss from the ocean surface across the subpolar gyre (Visbeck et al., 2003) and resulting in deeper winter mixed layers, particularly in the Labrador Sea (Sarafanov, 2009; Kieke et al., 2007).

In this paper, we consider how, and to what extent, NAO-mediated forcing of the ocean surface impacts the ventilation of the deep Atlantic Ocean. In particular, we explore how the interplay of atmospheric forcing and the ocean circulation imparts interannual variability to the transport of mixed layer properties into the ocean subsurface: an interannual Demon.

2 Numerical simulation and Lagrangian trajectory analysis

We tackle this problem using trajectory analysis in an eddy-permitting, forced ocean-sea-ice model. The numerical simulation and Lagrangian trajectory experiments are the same as those described in MacGilchrist et al. (2020). Here, we summarize the key points and refer the reader to that previous work for more details, as well as for comparison of the model with observations in the high-latitude North Atlantic.

The numerical simulation is a global implementation of the Nucleus for European Modelling of the Ocean (NEMO) model (Madec, 2014). The ORCA025 configuration is used, which has a grid resolution of $1/4^\circ$ ($\sim 27.75\,\mathrm{km}$ at the equator, refined at high latitudes) and 75 uneven vertical levels. The ocean model is coupled to a sea-ice model, LIM2 (Bouillon et al., 2009).

The simulation runs from 1958 to 2015, and is forced with the historical atmospheric reanalysis: 'Drakkar Forcing Set 5', which is an updated version of the fields described in Brodeau et al. (2010). The simulation is initialised from rest with temperature and salinity from the Levitus climatological hydrography (Levitus et al., 1998). We do not include the first 18 years of the simulation in our analysis, when the adjustment of the ocean state to the initial conditions is the largest.

Trajectories are evaluated "offline" using the Lagrangian analysis tool, Ariane (Blanke & Raynaud, 1997). The model velocity and hydrographic fields (output as 5-day means) are assumed to be piece-wise stationary, changing discretely every 5 days. No attempt is made to parameterize sub-grid scale physics in the trajectories (van Sebille et al., 2018). Although the simulation is global, we restrict our Lagrangian experiments to the Atlantic sector, the extent of which can be seen in Figure 1.

We evaluate backwards-in-time trajectories from a model-defined North Atlantic Deep Water (NADW) with γ^n between 27.7 and 28.0 (see details and discussion in MacGilchrist et al., 2020), where γ^n is calculated according to the empirical formulation of McDougall and Jackett (2005). Particles are initialized at each model tracer point (located in the centre of the grid cell) at the end of September every year between 1976 and 2015. Each particle is assumed to be representative of the grid-cell volume in which it is initialized. Trajectories are evaluated backwards in time until reaching the base of the mixed layer, defined as a neutral density within 0.01 of the density at $10\,m$, following Thomas et al. (2015). Our primary results are insensitive to this definition of mixed layer depth.

To determine the interannual variability of ventilation, we first calculate the time-mean age distribution of the model NADW, achieved by averaging the distribution determined for each of the initialization years between 1976 and 2015. Then, we subtract that mean distribution from the age distribution in 2015, leaving age distribution anomaly at the end of the simulation. An anomalously large amount of 20 year old water in 2015 signals an anomalously large amount of water retained in the subsurface due to ventilation in 1995. We normalize by the mean age distribution to account for re-entrainment of the watermass over time.

3 Results

3.1 Stommel's Demon in NADW

Stommel's Demon was shown to operate in the ventilation of the subtropical thermocline (Williams et al., 1995). However, it is not immediately intuitive that such a process operates in the subpolar gyres. In these regions, the time-mean, depth-integrated flow in the basin interior, away from lateral boundaries, moves water poleward — back towards the region of deep mixed layers. Furthermore, substantial freshwater input (from glacial and sea-ice melt, as well as river run-off from the Arctic) and deep convective events combine to ensure that isopycnal outcrop migration does not occur in a strictly meridional fashion. Consequently, water subducted into NADW in summer could feasibly evade re-entrainment, dependent on its subsurface pathway (*e.g* transported southward in the western boundary current).

The month in which ventilated NADW is subducted from the mixed layer is shown in Figure 1. In panel (a) we show the month of subduction in each grid cell, averaged over the depth of NADW. The dominance of light and dark green illustrates that the majority of ventilation arises from subduction occurring in March and April, confirmed by the volumetric histogram in panel (b), and revealing that, as noted by Williams et al. (1995) for the subtropics, Stommel's Demon functions similarly in the high-latitudes. The histogram further shows that, although the peak is in late winter, ventilation of NADW takes place over a broad range of winter months, from December through May.

The dashed line in Figure 1b shows a probability distribution for the timing of the deepest mixed layers across the high-latitude North Atlantic domain. Throughout the year there is is a strikingly consistent lag of approximately one month between the timing of deepest mixed layers and that of subduction. MacGilchrist et al. (2020) noted that the majority of NADW ventilation occurs via subduction over a relatively narrow region in the Labrador Sea boundary current. In this region, the deepest mixed layers occur slightly later in the year than they do in the open ocean subpolar gyre, perhaps explaining part of the shift between the two curves in Figure 1b and emphasizing that the *location* of subduction is a crucial component of ventilation, in addition to the timing.

3.2 An interannual Demon

The normalized anomaly in the age distribution of NADW, which we adopt as a proxy for ventilation variability (see Section 2), is shown in Figure 2a (orange bars). The time-mean age distribution is also shown (green line), for which we can note the long-timescale decline in volume with increasing age, indicative of a slow erosion of the watermass as it is mixed diabatically or returned to the mixed layer. The interannual signal is strong, varying by as much as 100% of the mean (a normalized anomaly value of 1).

We wish to understand how variability in ventilation is related to atmospheric forcing of the upper ocean. In panel (b), we show the NAO index from Hurrell (1995, red and blue bars) as well as the anomaly in the integrated volume of the mixed layer. As

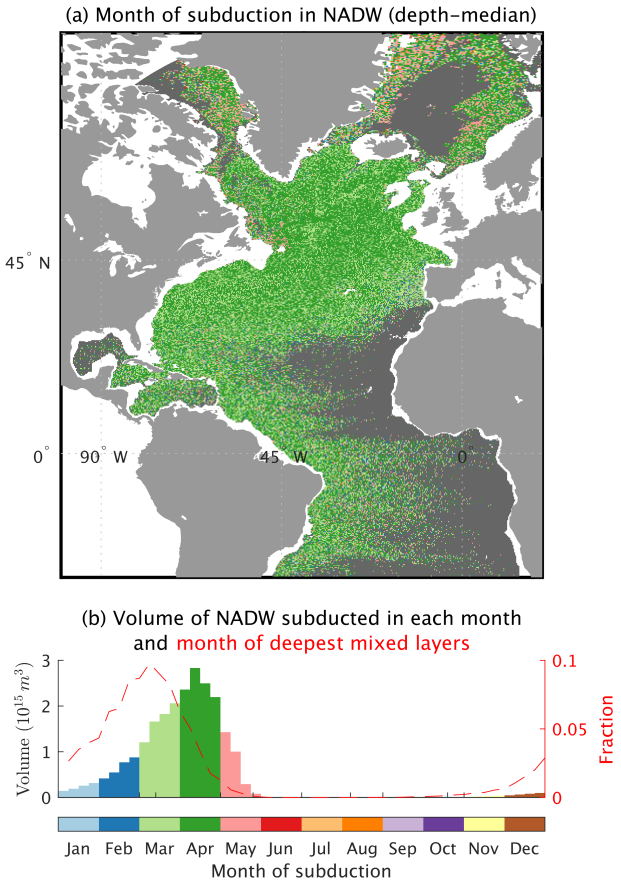

Figure 1. (a) Depth-median month of subduction for ventilated NADW in 2015. Dark gray indicates regions unventilated during the simulation. (b) Distribution of the month of subduction (colored bars; volumetric distribution derived from trajectories) and the month of deepest mixed layers (red dashed line; distribution of surface area fraction derived from the Eulerian fields). The dashed curve is evaluated by first determining the timing of the deepest mixed layer over the course of each year for each grid cell in the high-latitude North Atlantic (North of $40^{\circ}N$). A histogram is taken over all years and across all grid cells and the surface area occupied by each month is divided by the total surface area. Thus, the fraction denotes the probability that, for a given location and a given year, the deepest mixed layer occurred during that month.

expected (Visbeck et al., 2003), these two are well-correlated, indicating that changes in the atmospheric state have an impact on the depth of the upper ocean mixed layer.

Some variability in atmospheric forcing (Figure 2b) is translated to the ventilation anomalies (Figure 2a), at least in the sense that broad periods of positive NAO appear to match times of anomalously large ventilation (*e.g.* the 1990s). However, it is evident that the ventilation anomalies do not entirely match up with anomalies in the atmospheric state or upper ocean. This suggests that ventilation variability is also mediated by upper ocean dynamics.

Linear regression reveals that, as anticipated from Figure 2b, the volume of water present in the mixed layer in each year is well-correlated with the NAO ($R^2 = 0.41$). However, that correlation is eroded (to $R^2 = 0.14$) when considering only the amount of that water left in the subsurface following re-entrainment in the subsequent winter. In contrast, correlation between the final ventilation anomaly (Figure 2a) and the volume subducted each year is improved following re-entrainment (from $R^2 = 0.61$ to $R^2 = 0.85$). Such correlations show that while ventilation anomalies are initially established by atmospheric forcing variability, they are confounded by variations in the re-entrainment of water from year-to-year. That is, an interannual Demon mediates the years in which atmospheric forcing anomalies are "felt" by the deep ocean.

Of course, the deep mixed layers in any given year and the re-entrainment in the following year are *both* a result of atmospheric forcing, since re-entrainment itself is dependent on the subsequent year's mixed layer depth (with deeper mixed layers entraining more water). What is apparent here is that ventilation anomalies have a *memory* of at least 2 years of atmospheric forcing, manifest in the varying depth of the winter mixed layer. The dotted line in Figure 2a is a reconstruction of the ventilation anomaly based on mixed layer depth anomalies in each year and in the subsequent year; that is, representing ventilation as a forwards-in-time AR1 process. The reconstruction does a reasonable job in most years, and we find that the cumulative error is approximately halved compared to an equivalent reconstruction for an AR0 process (ventilation anomaly dependent only on the mixed layer depth anomaly in each year). Failing to account for the time-varying deep winter mixed layer thus results in the accumulation of errors in estimating ventilation to the ocean interior.

Two time periods (the early 1990s and late 2000s) provide particularly clear examples of the mediation of ventilation by atmospheric forcing variability. During the 1990s, there was a consistently strong, positive NAO, accompanied by deep winter mixed layers (Figure 2b). However, substantial positive ventilation anomalies are only present in the later years (Figure 2a), after 1993, and largest in the final year (1995), just before the NAO moved back into a negative phase. Likewise in 2008 and 2009, the ventilation anomaly peaks in the year following the transition to a negative NAO.

3.3 Deep convection and the open-ocean Demon

MacGilchrist et al. (2020) note that almost all of the ventilation in this simulation occurs in the boundary current of the Labrador Sea. We might question then, whether it is also in this region that the Demon operates, or whether the signal arises from deep convection in the central Labrador Sea.

Figure 3a shows the ventilation anomaly (as in Figure 2a) now separated by the bathymetric depth in the region where the particles left the mixed layer — as a proxy for whether the subduction occured in the boundary current (shallower than 3000 m bathymetric depth) or in the open ocean (deeper than 3000 m bathymetric depth). Anomalies associated with subduction in the boundary current make a broadly consistent contribution over time. On the other hand, major excursions are the result of anomalies in

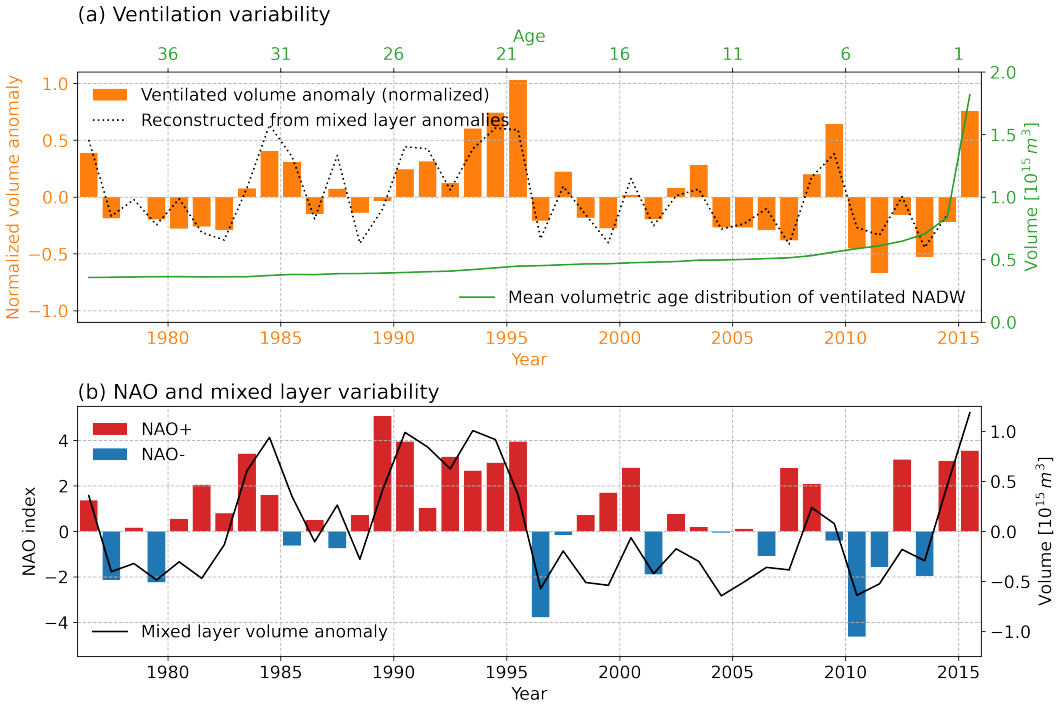

Figure 2. (a) Ventilation variability, as derived from the Lagrangian experiments. Green line is the mean age distribution of NADW from a number of different initialization years (see Section 2). Orange bars are the normalized anomaly around this mean age distribution for the initialization in 2015, which we take as a proxy for the ventilation anomaly in each year (*e.g.* + anomaly in 20 year old water implies + anomaly in 1995 ventilation, etc.). The dotted line is a reconstruction of the ventilation anomaly using multi-linear regression of mixed layer anomalies in the year itself and in the following year. (b) Atmospheric forcing and upper ocean response. Red and blue bars are the DJFM NAO index from Hurrell (1995). The solid line is the anomaly in the volume of the late winter mean mixed layer (*i.e.*, the volume of water that is within 0.01 of the surface density above it).

the open ocean, particularly forming the dominant contribution to the large anomalies in the 1990s.

A similar picture emerges when we consider the density class in which the ventilation anomalies appear. Figure 3b again shows the ventilation anomaly from Figure 2, here split by the density of the water at the end of the simulation. Anomalies prior to the mid-1990s appear in the densest density classes, and latterly shift towards mid-range and lighter densities. As noted in MacGilchrist et al. (2020), denser waters are preferentially subducted in the central Labrador Sea. Anomalies in the densest water masses are crucial in establishing the large positive deviations in the early part of the time-series and negative anomalies thereafter, interspersed with large positive anomalies in the intermediate classes. This apparent shift in the ventilation of the densest water masses is consistent with observed changes in the central Labrador Sea, for which the mid-1990s marked a shift in the formation of Labrador Sea Water (Kieke et al., 2007).

To return again to the relation between ventilation and surface forcing variability, we consider the surface-forced watermass transformation (Walin, 1982; Groeskamp et al., 2019). This is evaluated as the divergence of the integrated surface density flux within

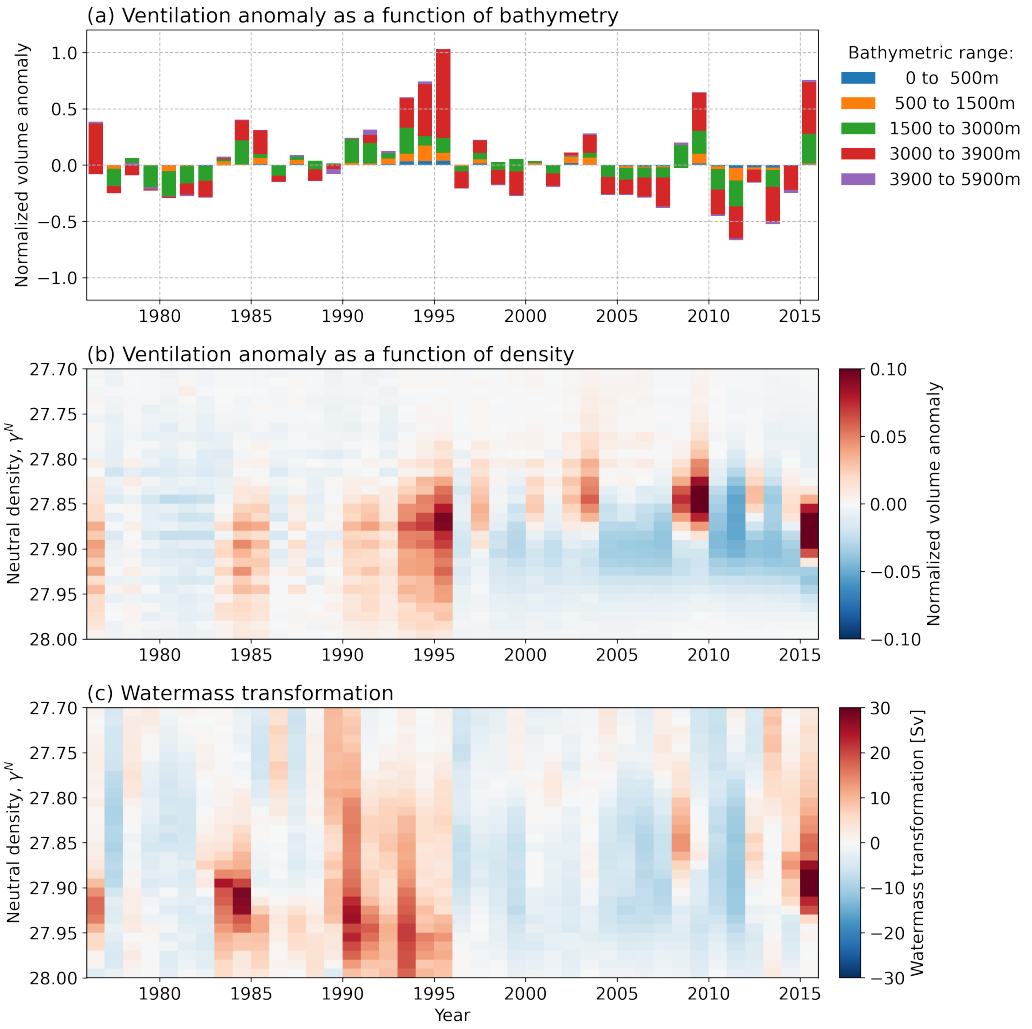

Figure 3. (a) Normalized ventilation anomaly (as in Figure 2a) separated according to the bathymetric contour over which subduction took place. (b) Normalized ventilation anomaly as a function of the neutral density of the water in September 2015 (simulation end). (c) Surface watermass transformation anomaly as a function of neutral density.

density bins of width $\Delta\gamma^n = 0.01$ across the North Atlantic domain, and reveals the transport of water across each density contour due to surface buoyancy forcing. We see in Figure 3c that the surface-forced transformation exhibits variability that is broadly consistent with that of ventilation, particularly on a time-scale consistent with that of the NAO (Figure 2). Noting again that the ventilation anomalies are evaluated only from the Lagrangian pathways of the model, it is striking that they should exhibit such clear memory of the surface forcing even to the end of the simulation and in the presence of the substantial subsurface mixing MacGilchrist et al. (2020). Closer consideration of Figure 3 reveals that ventilation anomalies exhibit deviations from variability imparted purely by the surface forcing, consistent with our impression from Figure 2. Maxima in ventilation in each density class arise *after* periods of sustained transformation anomalies (see, for example, the mid-1980s, mid-1990s and late 2000s), indicative of the interannual Demon at work.

4 Conclusions

Ventilation of the deep Atlantic occurs in late winter (Figure 1) and exhibits substantial variability on interannual and longer time-scales (Figure 2). Variability in atmospheric forcing associated with the NAO imparts a multi-annual (3- to 7-year) timescale on ocean ventilation through its impact on mixed layer depth. However, variations in the fraction of water that is re-entrained each year imparts an additional signature on the subsurface ocean (Figures 2 and 3). That is, water from particular years, selected for by changes in the depth of the late-winter mixed-layer and the pace of escape from the subduction location, preferentially ventilates the deep Atlantic: a process we call the "interannual Demon" by analogy with Stommel's 1979 paper on the seasonal Demon.

We illustrate the operation of the interannual Demon in Figure 4. Borrowing from schematic representations of Williams et al. (1995), we follow the Lagrangian evolution of water columns as they move progressively away from, or "escape", regions of deepest mixed layers. We consider two regimes: one in which that escape is slow and one in which it is fast; manifest in the extent to which the winter mixed layer shallows year-on-year under constant forcing conditions (gray lines). As an illustrative example, we consider variable interannual forcing (red lines) consisting of two years of progressively more positive NAO followed by a year of negative NAO. Along the slow escape pathway, the deepening of the mixed layer associated with the second year of positive NAO exceeds the natural shoaling of the mixed layer due to the water column's lateral displacement. Consequently, all of the water that leaves the mixed layer after the first winter is re-entrained the following year. No signature of ventilation from the first year is thus retained in the ocean subsurface, despite the positive NAO anomaly and deeper-than-normal mixed layer in that year. In this way, we can see how interannual variability mediates the passage of water into the subsurface ocean. In contrast, along the fast escape pathway, the natural shoaling of the mixed layer far exceeds the forcing-derived deepening of the winter mixed layer in the second year, allowing water subducted in the first year to remain in the subsurface. Thus, the pathway of newly ventilated water is a critical determinant for the influence of atmospheric variability and the operation of an interannual Demon.

As well as illustrating the impact of a time-varying mixed layer depth on ocean ventilation, the interannual demon has important practical implications. In particular, it is common to adopt the late-winter mixed layer depth and its year-to-year variation as a proxy for ocean ventilation and its variability (Boe et al., 2009; Li et al., 2016; Heuz, 2017). That perspective ignores the impact of an interannual Demon mediating the translation of surface variability into the subsurface ocean. We noted in Section 3.2 that this leads to a cumulative error in the estimation of ventilated volume. More appropriate, at least in this case for the North Atlantic, is to construct a model for ventilation that incorporates interannual changes in late-winter mixed layer depth (Figure 2a).

Although we have focused our analysis on the high-latitude North Atlantic, the interannual Demon could be operating across the global ocean. Based on our analysis, it is likely to be operating where the year-on-year changes in winter mixed layer depth exceed, or come close to, the change of the mean winter mixed layer depth over the lateral annual displacement of the fluid column (Figure 4). In the case of the North Atlantic, this is intricately connected to the occurrence of deep convection and the cyclonic circulation within the open-ocean Labrador Sea. Other potential locations then include the high-latitude Southern Ocean where convective events are thought to occur only sporadically (Killworth, 1983; Bernardello et al., 2014). Alternatively, mode and intermediate waters in the Southern Ocean, whose formation regions display substantial year-on-year variability in mixed layer depth and formation volume (Kolodziejczyk & Llovel, 2019; Qu et al., 2020), might also be good candidates for the operation of an interannual Demon.

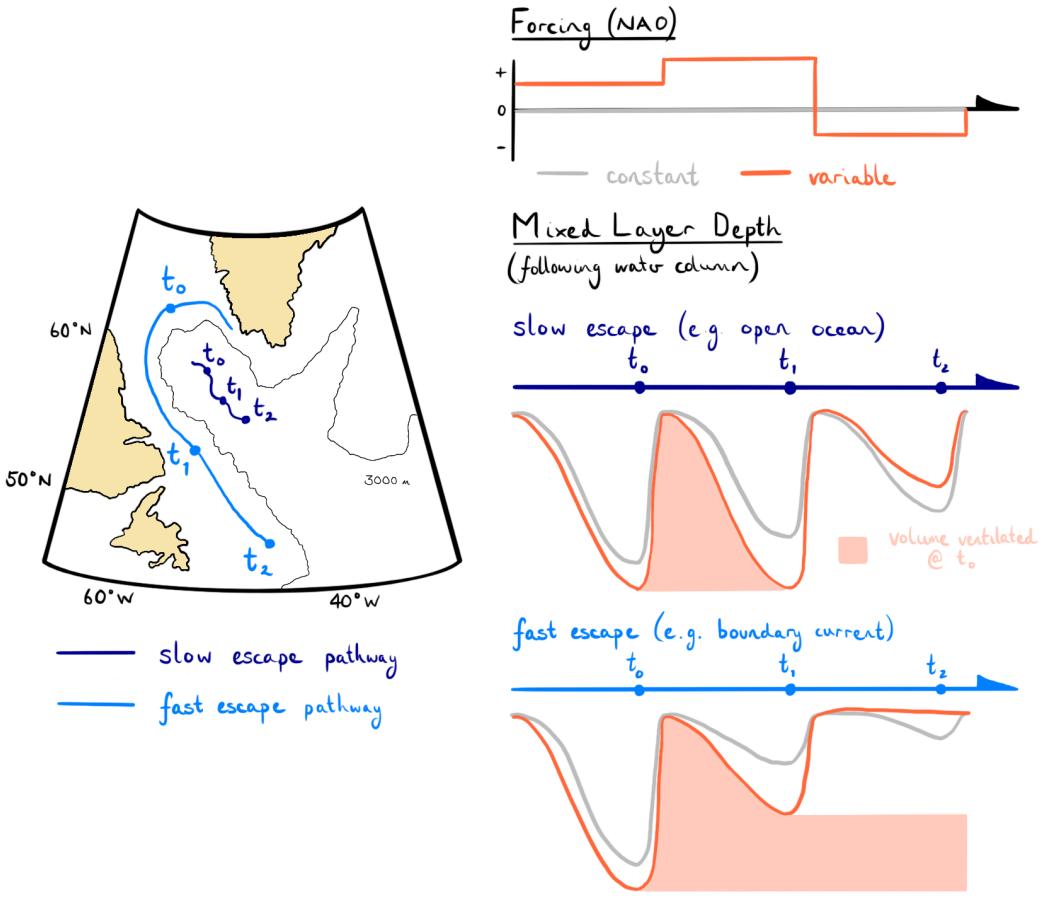

Figure 4. Schematic illustration of the operation of an interannual Demon, and the dependence on the speed at which newly subducted water moves away from the region of deep mixed layers and hence evades re-entrainment. On the left, we show two idealized pathways of water columns exiting the Labrador Sea. One pathway corresponds to transport in the central, open-ocean region (dark blue), while the other corresponds to transport via the boundary current (light blue). The positions of the columns in late winter of successive years are labeled t_i. On the right, we show the corresponding evolution of the mixed layer depth following these two water columns under constant forcing (gray lines) and variable forcing (red lines). The pattern of these forcings is shown on the top right, represented as idealized variations of the NAO. For the variable forcing case, we keep track of the water ventilated during the first winter (t_0), represented by the pink patch.

Finally, we have noted that the interannual Demon operates effectively in the open-ocean Labrador Sea because water there escapes only slowly and thus is frequently returned to the mixed layer. Such persistent re-ventilation, however, could actually increase the uptake and sequestration of certain atmospheric tracers. Carbon dioxide has a long equilibration timescale (between 6 and 18 months Jones et al., 2014) meaning that maximal exchange between the atmosphere and ocean requires water to be exposed to the atmosphere for more than a year. The interannual Demon might thus enhance the uptake of carbon in the open ocean Labrador Sea, since waters that eventually permanently subduct are likely to have had more time to reach equilibrium. It could thus be the case that the Demon is partly responsible for establishing the location and efficiency of anthropogenic carbon uptake.

Acronyms

NADW North Atlantic Deep Water

Acknowledgments

Code for reproducing the figures presented here is available on GitHub (github.com/gmacgilchrist; in repositories 'nadw' for Figure 1 and 'draw_figs_nadw' for Figures 2 and 3). The NEMO Ocean Model core is available at https://forge.ipsl.jussieu.fr/nemo/chrome/site/doc/NEMO/guide/html/install.html. The Lagrangian trajectory calculation software, Ariane, is available at https://stockage.univ-brest.fr/ grima/Ariane/. Model output used in this study can be obtained upon request to CL (camille.lique@ifremer.fr). GM is supported through NSFs Southern Ocean Carbon and Climate Observations and Modeling (SOCCOM) Project under the NSF Award PLR-1425989, with additional support from NOAA and NASA. HJ and DM were supported by the UK Natural Environment Research Council OSNAP project (NE/K010948/1). CL was supported by the project MEDLEY funded by JPI Climate and JPI Oceans. The hindcast was carried out within the European Drakkar project, and the model outputs were kindly provided by J.M Molines and C. Talandier. We used the computational tool Ariane developed by B. Blanke and N. Grima, who also provided support and advice on its use.

References

Bernardello, R., Marinov, I., & Palter, J. (2014). Impact of weddell sea deep convection on natural and anthropogenic carbon in a climate model. *Geophysical*.

Blanke, B., & Raynaud, S. (1997). Kinematics of the pacific equatorial undercurrent: An eulerian and lagrangian approach from gcm results. *Journal of Physical Oceanography*, *27*(6), 10381053.

Boer, A. D., Sigman, D., & Toggweiler, J. (2007). Effect of global ocean temperature change on deep ocean ventilation. .

Bouillon, S., Morales Maqueda, M. A., Legat, V., & Fichefet, T. (2009). An elastic-viscous-plastic sea ice model formulated on arakawa b and c grids. *Ocean Modelling*, *27*(3-4), 174184.

Boe, J., Hall, A., & Qu, X. (2009). Deep ocean heat uptake as a major source of spread in transient climate change simulations. *Geophysical Research Letters*, *36*(22), 15.

Brodeau, L., Barnier, B., Treguier, A. M., Penduff, T., & Gulev, S. (2010). An era40-based atmospheric forcing for global ocean circulation models. *Ocean Modelling*, *31*(3-4), 88104.

DeVries, T., & Primeau, F. (2011). Dynamically and observationally constrained estimates of water-mass distributions and ages in the global ocean. *Journal of Physical Oceanography*, *41*(12), 23812401.

Gebbie, G., & Huybers, P. (2012). The mean age of ocean waters inferred from radiocarbon observations: Sensitivity to surface sources and accounting for mixing histories. *Journal of Physical Oceanography*, *42*(2), 291305.

Groeskamp, S., Griffies, S., & Iudicone, D. (2019). The water mass transformation framework for ocean physics and biogeochemistry. *Annual review of*.

Heuz, C. (2017). North atlantic deep water formation and amoc in cmip5 models. *Ocean Science*.

Hurrell, J. W. (1995). Decadal trends in the north atlantic oscillation: regional temperatures and precipitation. *Science*, *269*(5224), 676679.

Hurrell, J. W., & Deser, C. (2010). North atlantic climate variability: the role of the north atlantic oscillation. *Journal of marine systems*, *79*(3-4), 231244.

Iselin, C. O. (1939). The influence of vertical and lateral turbulence on the characteristics of the waters at mid-depths. *Eos, Transactions American Geophysical Union*, *20*(3), 414417.

Jones, D., Ito, T., & Takano, Y. (2014). Spatial and seasonal variability of the air-sea equilibration timescale of carbon dioxide. *Global Biogeochemical*.

Katavouta, A., Williams, R., & Goodwin, P. (2019). The effect of ocean ventilation on the transient climate response to emissions. *Journal of Climate*.

Khatiwala, S., Primeau, F., & Hall, T. (2009). Reconstruction of the history of anthropogenic co 2 concentrations in the ocean. *Nature*, *462*(7271), 346349.

Kieke, D., Rhein, M., Stramma, L., Smethie, W. M., Bullister, J. L., & LeBel, D. A. (2007). Changes in the pool of labrador sea water in the subpolar north atlantic. *Geophysical Research Letters*, *34*(6).

Killworth, P. (1983). Deep convection in the world ocean. *Reviews of Geophysics*.

Koelling, J., Wallace, D. W., Send, U., & Karstensen, J. (2017). Intense oceanic uptake of oxygen during 20142015 winter convection in the labrador sea. *Geophysical Research Letters*, *44*(15), 78557864.

Kolodziejczyk, N., & Llovel, W. (2019). Interannual variability of upper ocean water masses as inferred from argo array. *Journal of Geophysical*.

Levitus, S., Boyer, T., Conkright, M., Brien, T. O., Antonov, J., Stephens, C., ... Gelfeld, R. (1998). *Noaa atlas nesdis 18, world ocean database 1998*. Washington D.C.: U.S. Government Printing Office.

Li, H., Ilyina, T., Mller, W., & Sienz, F. (2016). Decadal predictions of the north atlantic co 2 uptake. *Nature communications*.

Luyten, J., Pedlosky, J., & Stommel, H. (1983). The ventilated thermocline. *Journal of Physical Oceanography*, *13*(2), 292309.

MacGilchrist, G., Johnson, H., & Marshall, D. (2020). Locations and mechanisms of ocean ventilation in the high-latitude north atlantic in an eddy-permitting ocean model. *Journal of*.

Madec, G. (2014). *Nemo ocean engine*. Note du Pole de modelisation de lInstitut Pierre-Simon Laplace No 27.

Marshall, D. (1997). Subduction of water masses in an eddying ocean. *Journal of Marine Research*, *55*(2), 201222.

Marshall, D., & Marshall, J. (1995). On the thermodynamics of subduction. *Journal of physical oceanography*, *25*(1), 138151.

Marshall, J., Johnson, H., & Goodman, J. (2001). A study of the interaction of the north atlantic oscillation with ocean circulation. *Journal of Climate*, *14*(7), 13991421.

McDougall, T. J., & Jackett, D. R. (2005). The material derivative of neutral density. *Journal of Marine Research*, *63*, 159185.

Qiu, B., & Huang, R. X. (1995). Ventilation of the north atlantic and north pacific: subduction versus obduction. *Journal of Physical Oceanography*, *25*(10), 23742390.

Qu, T., Gao, S., & Fine, R. (2020). Variability of the sub-antarctic mode water subduction rate during the argo period. *Geophysical Research Letters*.

Rhein, M., Steinfeldt, R., Kieke, D., Stendardo, I., & Yashayaev, I. (2017). Ventilation variability of labrador sea water and its impact on oxygen and anthropogenic carbon: a review. *Philosophical Transactions of the Royal Society A: Mathematical, Physical and Engineering Sciences*, *375*(2102), 20160321.

Sarafanov, A. (2009). On the effect of the north atlantic oscillation on temperature and salinity of the subpolar north atlantic intermediate and deep waters. *ICES Journal of Marine Science*, *66*(7), 14481454.

Sarmiento, J. (1983). A tritium box model of the north atlantic thermocline. *Journal of Physical Oceanography*, *13*(7), 12691274.

Stommel, H. (1979). Determination of water mass properties of water pumped down from the ekman layer to the geostrophic flow below. *Proceedings of the National Academy of Sciences*, *76*(7), 30513055.

Thomas, M. D., Treguier, A.-m., Blanke, B., Deshayes, J., & Voldoire, A. (2015). A lagrangian method to isolate the impacts of mixed layer subduction on the meridional overturning circulation in a numerical model. *Journal of Climate*, *28*, 75037517.

van Sebille, E., Griffies, S. M., Abernathey, R. P., Adams, T. P., Berlo, P., Biastoch, A., ... Zika, J. D. (2018). Lagrangian ocean analysis : Fundamentals and practices. *Ocean Modelling*, *121*, 4975.

Visbeck, M., Chassignet, E. P., Curry, R. G., Delworth, T. L., Dickson, R. R., & Krahmann, G. (2003). The oceans response to north atlantic oscillation variability. In *The north atlantic oscillation: Climatic significance and environmental impact* (p. 113-146). American Geophysical Union.

Walin, G. (1982). On the relation between sea-surface heat flow and thermal circulation in the ocean. *Tellus*, *34*(2), 187195.

Williams, R. G. (1991). The role of the mixed layer in setting the potential vorticity of the main thermocline. *Journal of Physical Oceanography*, *21*(12), 18031814.

Williams, R. G., Marshall, J. C., & Spall, M. A. (1995). Does stommels mixed layer demon work. *Journal of Physical Oceanography*, *25*(12), 30893102.

Zanna, L., Khatiwala, S., Gregory, J. M., Ison, J., & Heimbach, P. (2019). Global reconstruction of historical ocean heat storage and transport. *Proceedings of the National Academy of Sciences*, *116*(4), 11261131.

Figure 2.

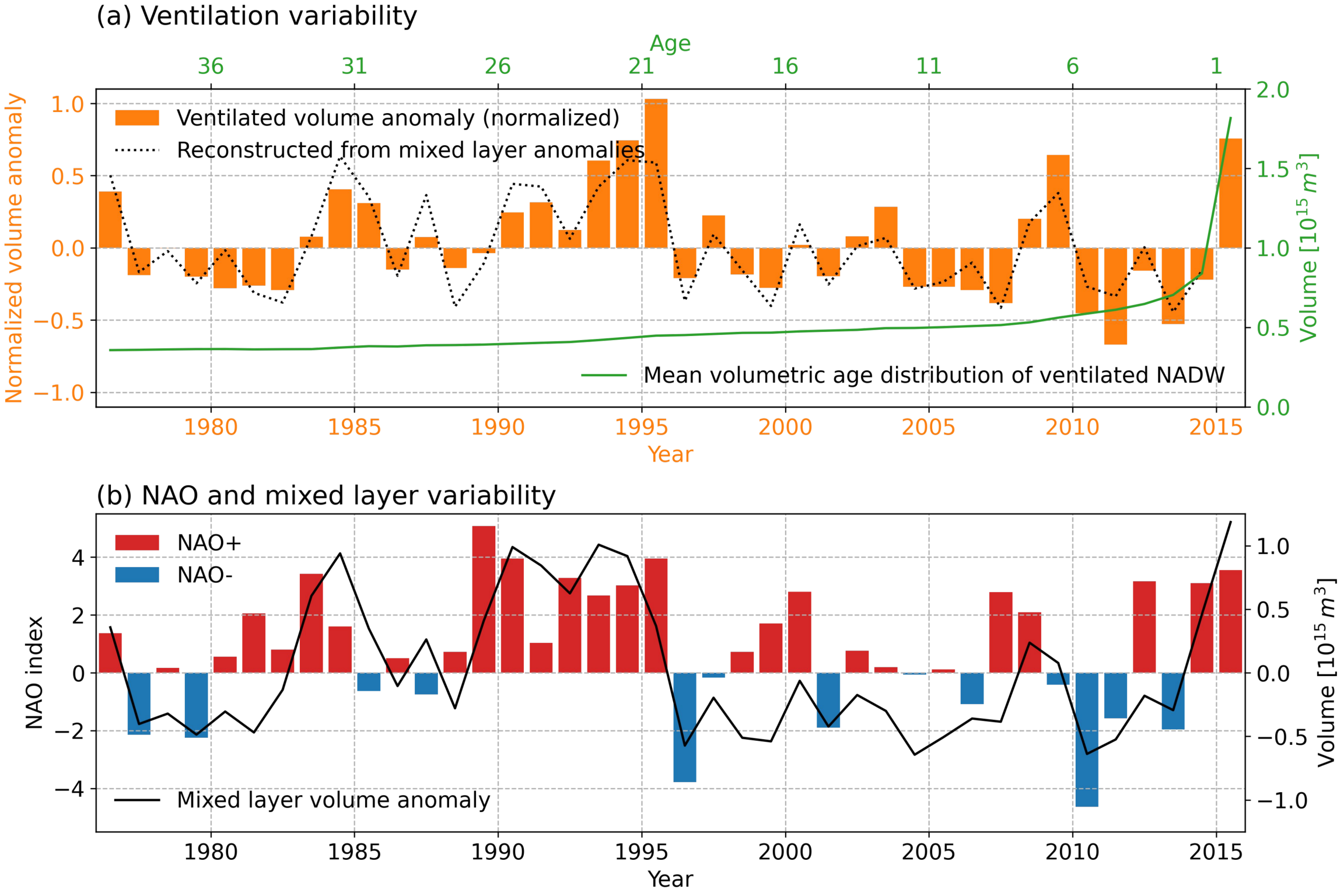
(a) Ventilation variability
Age
36
31
26
21
16
11
6
1
Normalized volume anomaly
1.0
0.5
0.0
−0.5
−1.0
Ventilated volume anomaly (normalized)
Reconstructed from mixed layer anomalies
Mean volumetric age distribution of ventilated NADW
Volume [10^{15} m^3]
2.0
1.5
1.0
0.5
0.0
1980
1985
1990
1995
2000
2005
2010
2015
Year
(b) NAO and mixed layer variability
NAO index
4
2
0
−2
−4
NAO+
NAO-
Mixed layer volume anomaly
Volume [10^{15} m^3]
1.0
0.5
0.0
−0.5
−1.0
1980
1985
1990
1995
2000
2005
2010
2015
Year

Figure 3.

(a) Ventilation anomaly as a function of bathymetry

Normalized volume anomaly

1.0
0.5
0.0
−0.5
−1.0

1980 1985 1990 1995 2000 2005 2010 2015

Bathymetric range:
0 to 500m
500 to 1500m
1500 to 3000m
3000 to 3900m
3900 to 5900m

(b) Ventilation anomaly as a function of density

Neutral density, γ^N

27.70
27.75
27.80
27.85
27.90
27.95
28.00

1980 1985 1990 1995 2000 2005 2010 2015

0.10
0.05
0.00
−0.05
−0.10
Normalized volume anomaly

(c) Watermass transformation

Neutral density, γ^N

27.70
27.75
27.80
27.85
27.90
27.95
28.00

1980 1985 1990 1995 2000 2005 2010 2015

Year

30
20
10
0
−10
−20
−30
Watermass transformation [Sv]

Figure 1.

(a) Month of subduction in NADW (depth-median)

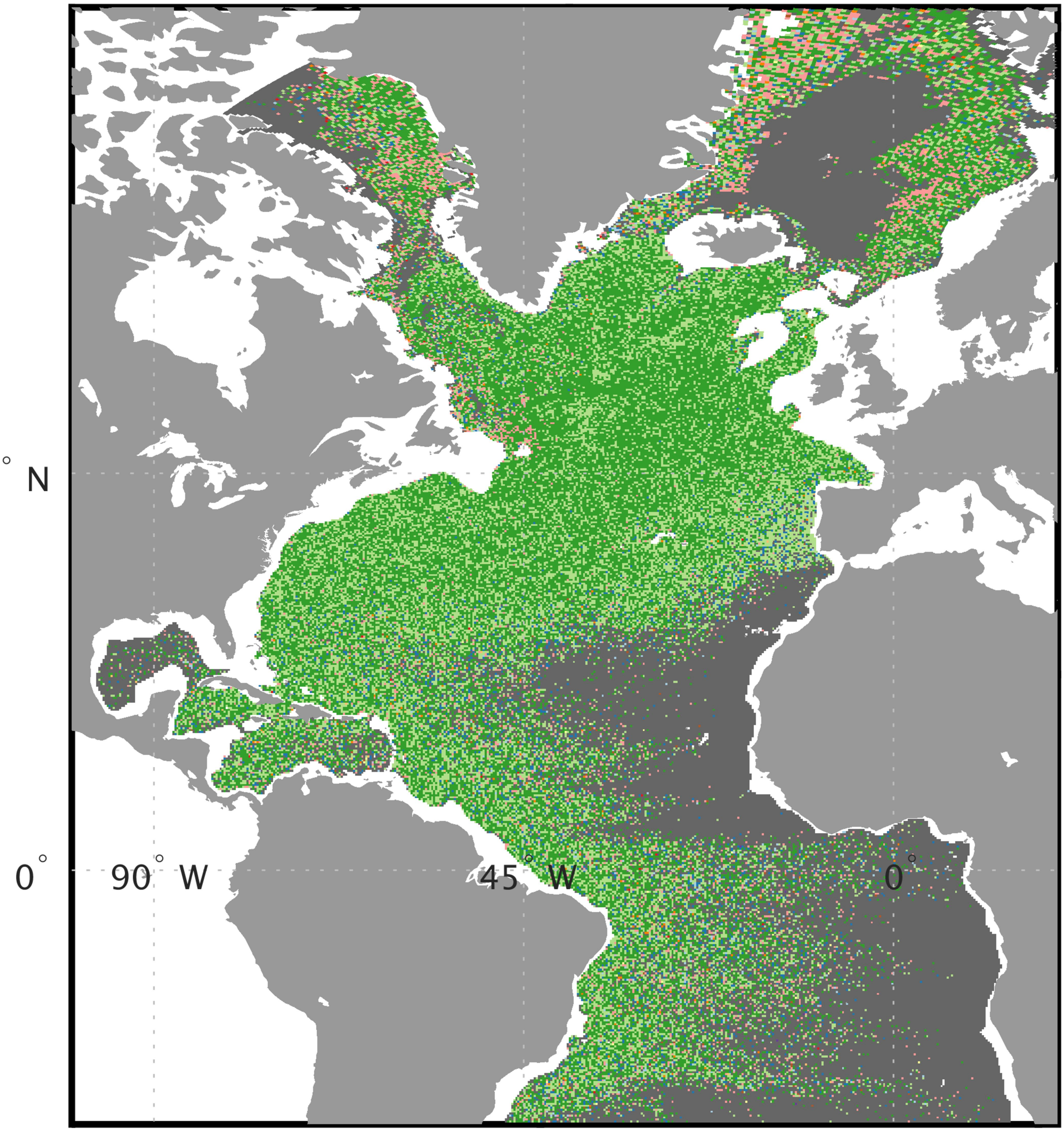

(b) Volume of NADW subducted in each month
and month of deepest mixed layers

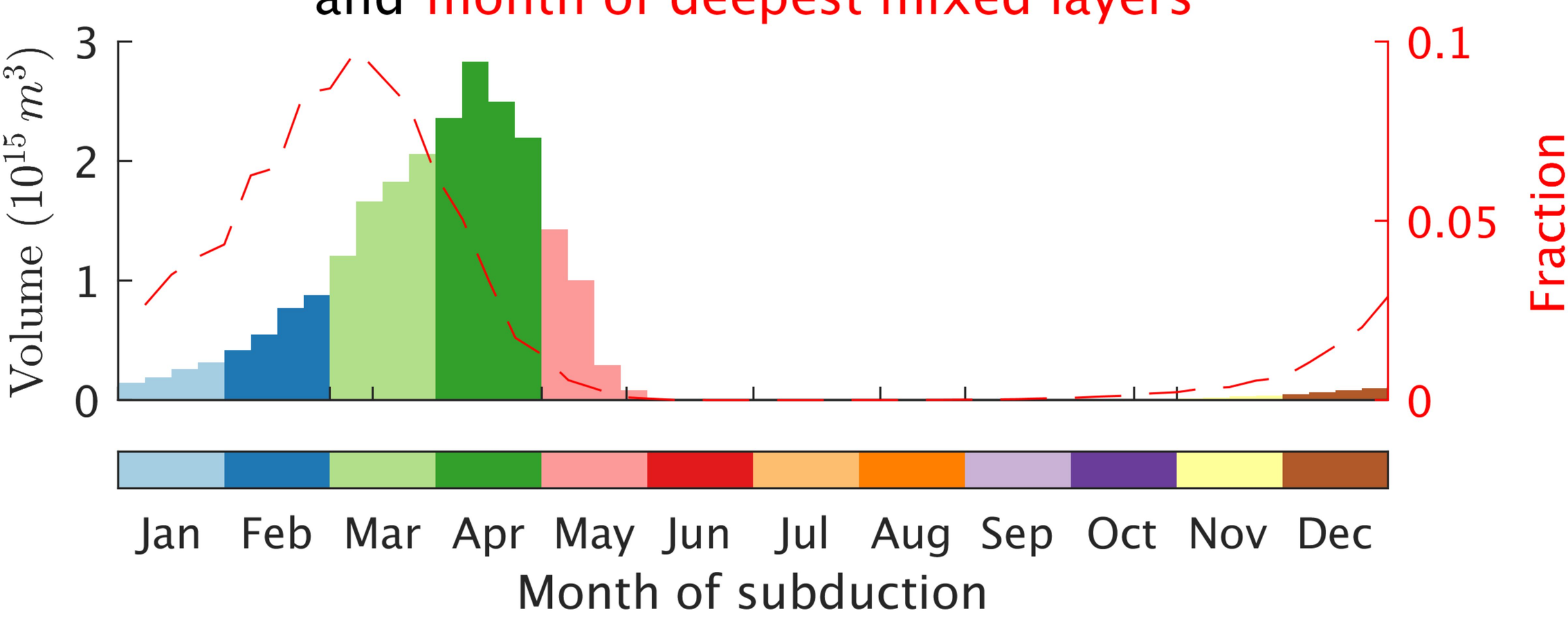

Figure 4.

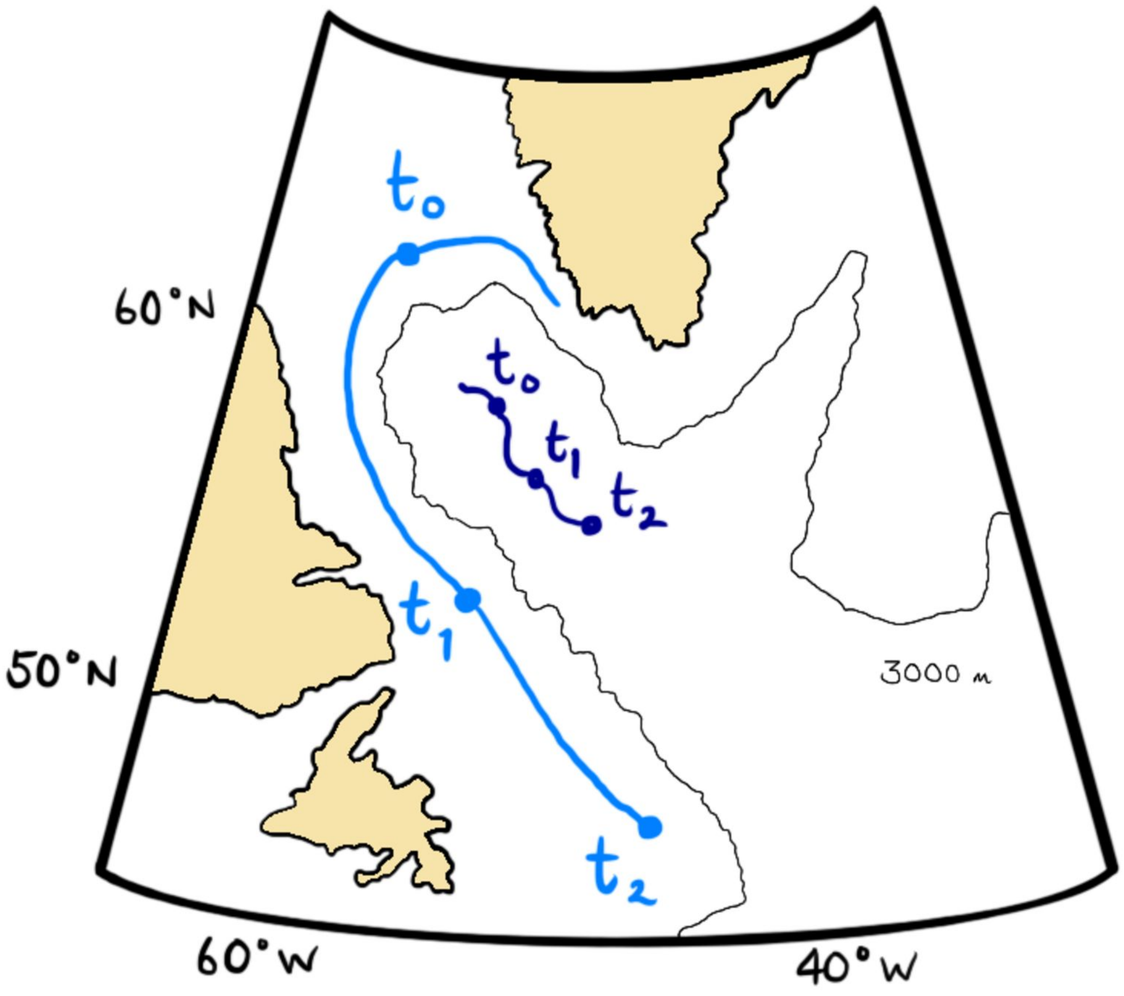

slow escape pathway

fast escape pathway

Forcing (NAO)

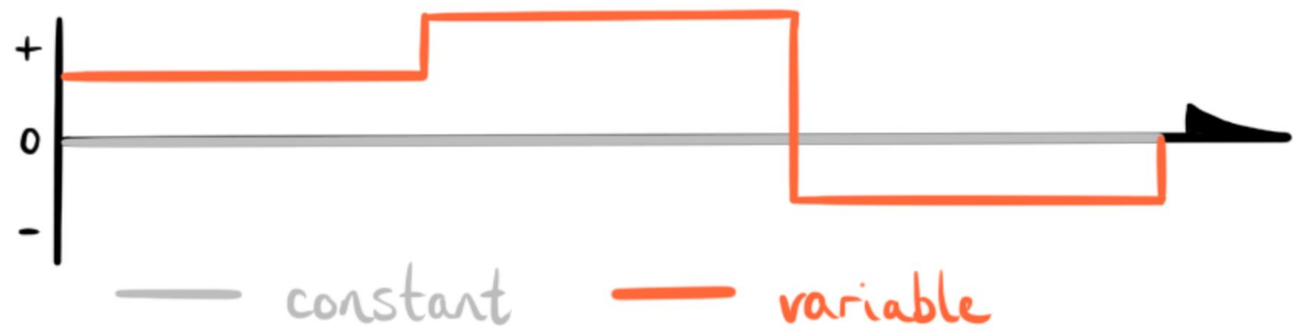

Mixed Layer Depth

(following water column)

slow escape (e.g. open ocean)

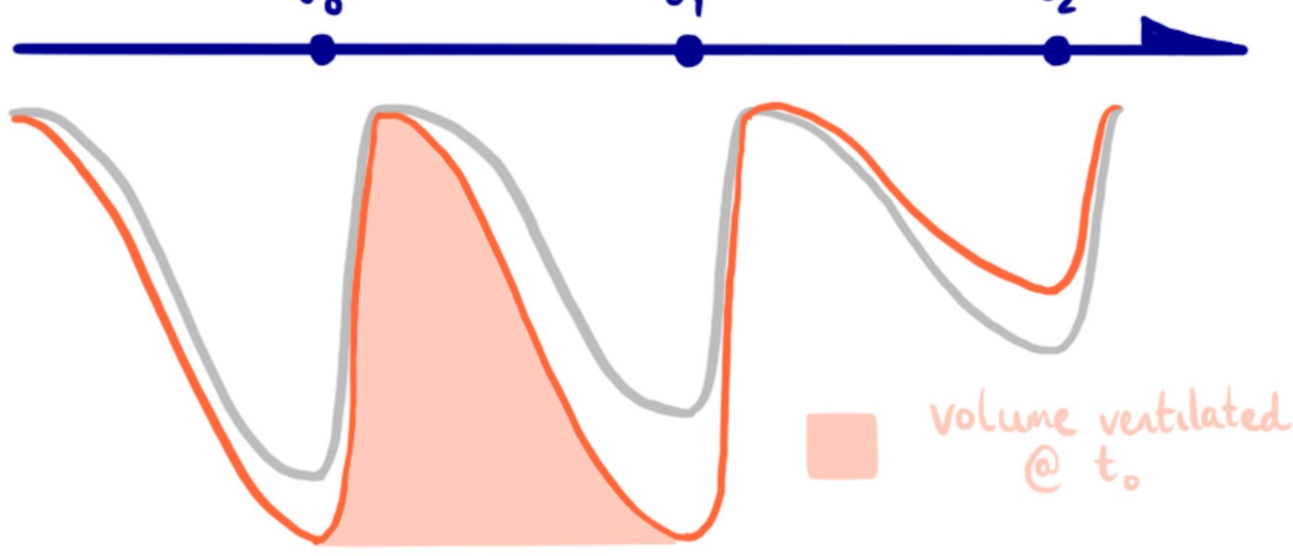

fast escape (e.g. boundary current)